Fragmentation of H_2^+ in strong 800-nm laser pulses: Initial-vibrational-state dependence

Bernold Feuerstein* and Uwe Thumm†
Department of Physics, Kansas State University, Manhattan, Kansas 66506
(Received 17 December 2002; published 15 April 2003)

The fragmentation of the H_2^+ molecular ion in 25-fs, 800-nm laser pulses in the intensity range 0.05–0.5 P W/cm^2 is investigated by means of wave-packet propagation calculations. We use a collinear reduced-dimensionality model that represents both the nuclear and electronic motion by one degree of freedom including non-Born-Oppenheimer couplings. In order to reproduce accurately the properties of the ''real'' three-dimensional molecule, we introduce a modified ''soft-core'' Coulomb potential with a softening function that depends on the internuclear distance. The analysis of the calculated flux of the outgoing wave packets allows us to obtain fragmentation probabilities and kinetic-energy spectra. Our results show that the relative probabilities for dissociation and Coulomb explosion depend critically on the initial vibrational state of the molecular ion.

DOI: 10.1103/PhysRevA.67.043405 PACS number(s): 33.80.Rv, 33.90.+h, 42.50.Hz

I. INTRODUCTION

This simplest molecule, the hydrogen molecular ion, is of fundamental interest in atomic and molecular physics. It constitutes a bound three-body Coulomb system which, in contrast to its atomic counterparts, the negative hydrogen ion and the helium atom, exhibits (if we neglect rotation) two time scales, the fast electronic motion (as scale) and the vibrational motion of the nuclei [femtosecond (fs) scale]. The interaction of this smallest molecule with strong fs laser pulses is of particular interest, since the pulse duration is comparable to the vibrational period (14 fs for H_2^+ in the vibrational ground state). Further, from a theoretical point of view, the simple structure of H_2^+ allows for a numerical solution of the time-dependent Schrödinger equation within reduced dimensionality models by using, e.g., standard Crank-Nicholson split-operator propagation techniques [1–7].

Interacting with a strong, linearly polarized laser field, H_2^+ exhibits two fragmentation channels, dissociation

$$H_2^+ + n\hbar\omega \rightarrow p + H, \tag{1}$$

and Coulomb explosion (CE)

$$H_2^+ + n'\hbar\omega \rightarrow p + p + e^-. \tag{2}$$

The fragmentation of H_2^+ in strong laser fields has been considered in numerous theoretical investigations emphasizing the influence of the two-center nature of the electronic potential on strong-field ionization [3,4,8–15]. Here, the laser-induced coupling of the lowest electronic states $1s\sigma_g$ and $2p\sigma_u$ results in a localization of the electron near one of the nuclei. The electron cloud oscillates between the nuclei and gives rise to dissociation of the molecule and to ''charge resonance enhanced ionization'' (CREI) at intermediate internuclear distances R between 5 and 10 a.u. [4,8,9].

Experimentally, the situation is more challenging since mostly neutral H_2 targets are available [16–22], such that the production and fragmentation of the molecular ion occur in the same laser pulse and are difficult to separate. It was shown that for 50-fs pulses, saturation of H_2^+ is never reached at any intensity [19]. Hence, there is a growing interest in molecular ions as targets which have been investigated in two recent experiments [23,24]. In this work, we consider the vibrational-state dependence of the fragmentation yields for the processes (1) and (2). The experimental data of Posthumus *et al.* [19] show that there is competition of dissociation and CREI for intensities around 10^{14} W/cm^2. We use wave-packet propagation calculations in a collinear 2×1D (one-dimensional) model to derive dissociation and CE probabilities and the corresponding kinetic-energy spectra for the fragments.

This paper is structured as follows. First, in Sec. II, we describe our theoretical model with emphasis on the effects of the reduced dimensionality on the potential curves of H_2^+. This section includes a discussion of the properties of the widely used ''soft-core'' (SC) Coulomb potential [25] for the electron-nucleus interaction (Sec. II A). In Sec. II B, we present an improved SC Coulomb potential which allows the exact reproduction of the 3D ground-state potential curve of H_2^+. Next, we provide kinetic-energy spectra by applying the recently proposed ''virtual detector'' method [26] to the laser-induced fragmentation of H_2^+. We present and discus the numerical results for the vibrational-state dependence of the fragmentation dynamics including the intensity dependence for two selected vibrational states (Sec. III). Our concluding remarks follow in Sec. IV. Atomic units are used throughout this paper, unless otherwise indicated.

II. THEORETICAL MODEL

For linearly polarized nonrelativistic laser fields considered here, only the coordinates parallel to the electric-field vector play an important role. Thus, in order to keep the computational effort at a reasonable level, we describe the molecular ion in a collinear model. This reduced-dimensionality model includes two coordinates, the elec-

*Electronic address: feuerstb@mpi-hd.mpg.de
†Electronic address: thumm@phys.ksu.edu

tronic coordinate z relative to the center of mass of the nuclei and the internuclear distance R. The model-inherent alignment of the molecule along the polarization axis is not a serious problem, since in a kinematically complete experiment fragmentation along this axis can be selected. We note that the model includes non-Born-Oppenheimer couplings between the electronic and nuclear motion. The solution of the time-dependent Schrödinger equation is formally given by the propagation of the initial wave function,

$$\Psi(z,R,t)=\exp\left[-i\int_0^t dt'\,\mathcal{H}(z,R,t')\right]\Psi(z,R,t=0) \quad (3)$$

with the Hamiltonian

$$\mathcal{H}(z,R,t)=\mathcal{T}_R+V_{nn}(R)+\mathcal{H}_{el}, \quad (4a)$$

$$\mathcal{H}_{el}=\mathcal{T}_z+V_{en}(z,R)+F(t)z. \quad (4b)$$

$\mathcal{T}_R$ and $\mathcal{T}_z$ are the kinetic-energy operators for the electronic and the nuclear motion. $V_{nn}(R)=1/R$ is the internuclear Coulomb potential and $V_{en}(z,R)$ the two-center Coulomb potential for the electron-nucleus interaction. The interaction of the electric component $F(t)$ of the laser field with the electron is given in dipole approximation in the length gauge. The propagation (3) is carried out numerically on a grid using the Crank-Nicholson split-operator method which provides unconditional numerical stability [27]. Here, for each time step Δt, the wave function at time $t+\Delta t$ is recursively given by

$$\Psi(t+\Delta t)=\exp[-\tfrac{1}{2}i\mathcal{T}_R\Delta t]\exp[-i(V_{nn}+\mathcal{H}_{el})\Delta t]\times\exp[-\tfrac{1}{2}i\mathcal{T}_R\Delta t]\Psi(t)+O(\Delta t^3). \quad (5)$$

In order to avoid the singularity of the Coulomb potential in 1D calculations, usually a SC Coulomb potential is introduced [3,25].

A. Soft-core Coulomb potential for H_2^+

Before we discus the application of the SC potential to the H_2^+ molecular ion, we briefly consider its basic properties. The SC Coulomb potential is given by

$$V_{\mathrm{SC}}(z)=\frac{-Q}{\sqrt{z^2+a^2}}. \quad (6)$$

Q describes the (effective) nuclear charge of the atom/ion, and a is a ''softening'' parameter which removes the singularity at $z=0$. For large z, this looks like a Coulomb potential $-Q/z$ whereas the behavior for small z resembles a harmonic-oscillator potential

$$V_{\mathrm{SC}}(z)=-Q/a+Qz^2/(2a^2)+O(z^3). \quad (7)$$

The parameter a can be adjusted in order to reproduce the correct ground-state energy. In principle, one could also change the parameter Q. However, this would lead to an unphysical asymptotic behavior of the potential, and Q would differ from the asymptotic charge seen by the electron at large distances z. For one-electron systems, such as hydrogenlike ions, it turns out that for each value of Q the parameter a has to be adjusted separately in order to reproduce the correct binding energy of the ground state.

In the case of H_2^+, the two-center potential requires a continuous adjustment of a while the internuclear distance R is changed. The two limiting cases are $R=0$ (He atom, $a=0.709$) and $R\to\infty$ (H atom, $a=1.415$). In their previous work, Kulander, Mies, and Schafer [3] suggested a softening function $a(R)$, but did not use it for their calculations. Instead, they keep $a=1$ fixed for all internuclear distances. They compare the basic properties of their 1D model molecule with known 3D results for the shape of the two lowest electronic state ($1s\sigma_g$ and $2p\sigma_u$) potential curves and the dipole matrix element $d_{ug}=\langle 2p\sigma_u|z|1s\sigma_g\rangle$ coupling these states. It has been shown [4,8,9] that these two states and their coupling are most important for the dynamics of H_2^+ in strong laser fields. The degeneracy of $1s\sigma_g$ and $2p\sigma_u$ electronic states enables charge localization at one nucleus and results in a diverging dipole moment which increases linearly with R. The shape of the potential curves also affects the positions of (avoided) crossings of the different $n\omega$ Floquet channels, corresponding to a net absorption of $n=1$, 2, or 3) photons [16]. Figure 1(a) shows these 1D dressed potential curves for a fixed softening parameter $a=1$ in comparison with the result of a full 3D calculation. We find the $1s\sigma_g$ curve in the 1D model from Ref. [3] shifted to larger R by 30% in the equilibrium distance whereas the $2p\sigma_u$ curves show a better overall agreement of the 1D and 3D calculations. The larger equilibrium distance R_0 in Kulander's model is crucial, since the ionization probability depends critically on the position of R_0 relative to the curve crossings. A comparison of the model molecular properties with the corresponding exact 3D values is given in Table I. The anharmonicity constant $\omega_e x_e$ is obtained by fitting the lowest vibrational energies in the $1s\sigma_g$ potential curve to the expression $E_v=\omega_e(v+\frac{1}{2})-\omega_e x_e(v+\frac{1}{2})^2$. Figure 2 shows the 1D and 3D values for the coupling dipole moment d_{ug} of the lowest electronic states as a function of R.

B. Improved soft-core Coulomb potential for H_2^+

Based on the idea of Kulander, Mies, and Schafer [3] to use a softening function $a(R)$, we now attempt to find a more realistic 1D model. The SC Coulomb potential (7) behaves like a harmonic-oscillator potential for small z. The parameter a determines simultaneously the depth $-Q/a$ and width of the potential. The width is proportional to $a/\sqrt{Q}$, i.e., it is given by the prefactor Q/a^2 of the quadratic term. Our idea is now to control depth and width of the SC Coulomb potential for H_2^+ independently in order to reproduce the exact $1s\sigma_g$ curve and, at the same time, to yield a reasonable agreement for $2p\sigma_u$. This modified SC Coulomb potential is given by

$$V_{\mathrm{SCmod}}(z)=\frac{-Q}{1/a-a/b+\sqrt{z^2+(a/b)^2}}, \quad (8)$$

with two parameters a and b. For small z we find

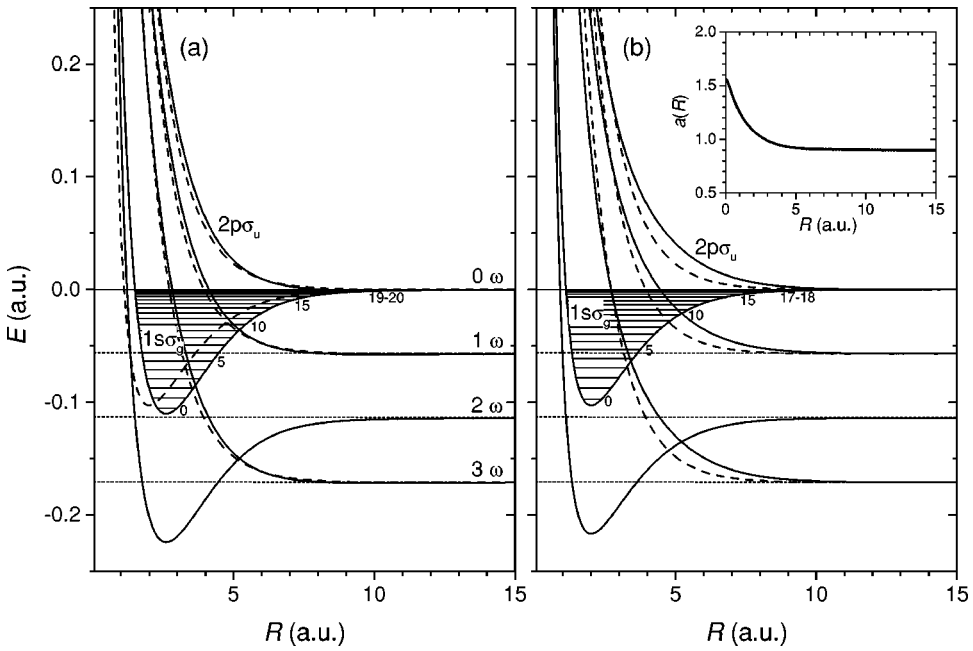

FIG. 1. Dressed $n\omega$ ($n=0,\ldots,3$) Floquet potential curves and vibrational energy levels for the two lowest electronic states $1s\sigma_g$ and $2p\sigma_u$ of H_2^+. Solid curves, 1D model molecule; dashed curves, full 3D result. (a) Model by Kulander, Mies, and Schafer [3] using the SC Coulomb potential (6) with a fixed softening parameter $a=1$. (b) Improved model (this work) based on the modified SC Coulomb potential (8) with the softening function $a(R)$ (shown in the inset).

$V_{\mathrm{SCmod}}(z)\approx -Q(a-\frac{1}{2}bz^2)$, whereas for large z the asymptotic behavior $-Q/z$ is unchanged. Using V_{SCmod}, the two-center model potential in Eq. (4) for H_2^+ ($Q=1$) takes the form

$$V_{en}(z,R)=\frac{-1}{1/a(R)-a(R)/b+\sqrt{z_-^2+[a(R)/b]^2}}+\frac{-1}{1/a(R)-a(R)/b+\sqrt{z_+^2+[a(R)/b]^2}},$$

$$z_\pm=z\pm R/2. \tag{9}$$

For a given value of b, the function $a(R)$ is adjusted to *exactly* reproduce the 3D potential curve of $1s\sigma_g$. b is a fixed parameter which determines the shape of the repulsive $2p\sigma_u$ curve. The result for $b=5$ in comparison with the 3D curves is shown in Fig. 1(b) with the function $a(R)$ given as an inset. There is still some difference between our 1D and the full 3D models for the $2p\sigma_u$ potential curve. A better agreement can be achieved for larger values of b but this makes the potential more and more cusplike at the position of the nuclei. This limits the value of b since for practicable grid spacings the numerical grid cannot resolve a very narrow potential cusp. We found that $b=5$ models the repulsive $2p\sigma_u$ potential curve well without causing spurious effects in the numerical propagation on the grid. Based on our modified SC Coulomb potential (9), we calculated the properties of our 1D model molecule. In comparison with the 1D SC Coulomb potential from Ref. [3], our results are in better agreement with the 3D data (see Fig. 1 and Table I). In

TABLE I. Properties of the 1D model molecule compared with the real 3D molecule (atomic units). R_0, equilibrium internuclear distance; D_e, dissociation energy; ω_e, ground-state frequency; $\omega_e x_e$, anharmonicity constant; I_p, ionization potential.

			1D model	
		3D result[a]	[3]	This work
R_0		2.0	2.6	2.0
D_e		0.103	0.11	0.103
ω_e		1.06×10^{-2}	9.93×10^{-3}	1.06×10^{-2}
$\omega_e x_e$		3.02×10^{-4}	2.02×10^{-4}	3.02×10^{-4}
$I_p(R_0)$		1.1	1.154	1.1
Number of bound states		19	21	19
1ω crossing	R	4.8	5.2	5.2
	v	9	9	10
3ω crossing	R	3.3	3.6	3.4
	v	3	2	4
1ω threshold		$v\geqslant5$	$v\geqslant6$	$v\geqslant5$

[a]Molecular constants from Ref. [28].

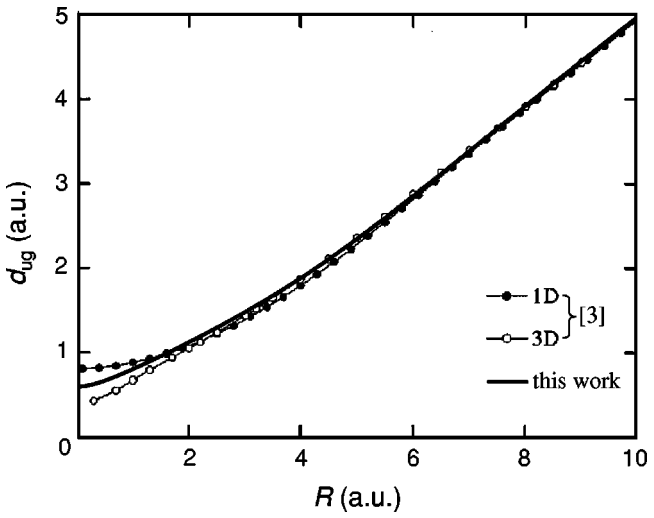

FIG. 2. Dipole coupling matrix element $d_{ug}=\langle 2p\sigma_u|z|1s\sigma_g\rangle$ for the lowest electronic sates of H_2^+. One-dimensional model calculation of this work compared with the former result (1D model and full 3D calculation) from Ref. [3].

addition, the dipole moment d_{ug} is slightly better reproduced than by the simple SC Coulomb potential (Fig. 2).

We note that by adjusting a softening function $a(R)$ only in a model potential $V(z,R)=-Q/\sqrt{z^2+a(R)^2}$, the $1s\sigma_g$ potential curve can also be exactly reproduced. However, the shape of the corresponding repulsive $2p\sigma_u$ curve is in quite poor agreement with the 3D result. This led us to introduce a second free parameter b in Eqs. (8) and (9).

C. Numerical propagation scheme

Our numerical grid extends from 0.05 to 30 in R with a spacing of 0.05 and from -45 to 45 in z with a spacing of 0.2. Absorbing regions using an optical potential are introduced in order to prevent the reflection of the outgoing wave packets at the border of the grid. We implemented this absorber as fourth-order optical potentials in z and R:

$$V_{\rm opt}(z,R)=-i[V_z(z)+V_R(R)], \tag{10a}$$

$$V_z(z)=\begin{cases}5[(-25-z)/20]^4, & z\leqslant -25\\ 5[(z-25)/20]^4, & z\geqslant 25\\ 0 & \text{otherwise,}\end{cases} \tag{10b}$$

$$V_R(R)=\begin{cases}0.05[(R-20)/10]^4, & R\geqslant 20\\ 0 & \text{otherwise.}\end{cases} \tag{10c}$$

The number of time steps per optical cycle is 1100. For each time step the norm of the total wave function within $0.05\leqslant R\leqslant 20$, $-25\leqslant z\leqslant 25$ is calculated. The outgoing current flux through the borders $z_{vd}=\pm 25$, $R_{vd}=20$ of this inner part of the grid is used to obtain differential and integrated data on the fragmentation process. If we write the outgoing wave packet in terms of a real amplitude A and a real phase ϕ,

$$\Psi(z,R,t)=A(z,R,t)\exp[i\phi(z,R,t)], \tag{11}$$

we find the current density

$$\mathbf{j}(z,R,t)=\frac{|A(z,R,t)|^2}{m}\nabla\phi(z,R,t). \tag{12}$$

Here, m is the mass of the particle. The dissociation yield D into the fragmentation channel (1) is given by the time-integrated nuclear flux in the R direction at R_{vd},

$$D(t)=\int_0^t dt'\int_{-z_{vd}}^{+z_{vd}} dz\, j_R(z,R_{vd},t'). \tag{13}$$

Removal of the electron leads to CE, the yield of which is given by the time-integrated electronic flux in the z direction at $z=\pm z_{vd}$,

$$\mathrm{C}(t)=\int_0^t dt'\int_{0.05}^{R_{vd}} dR\, j_z(z_{vd},R,t'). \tag{14}$$

We derive the nuclear momentum distribution for dissociation using the ''virtual detector'' method [26] and imagine virtual detectors for the nuclear and electronic flux at the positions R_{vd} and $\pm z_{vd}$ indicated above. At each time step t_i, we numerically calculate the gradient of ϕ at R_{vd} using a five-point formula for the momentum,

$$p_R^{(D)}(z,t_i)=\left.\frac{\partial}{\partial R}\right|_{R_{vd}}\phi(z,R,t_i). \tag{15}$$

Integration over z and binning of the momentum values for all times t_i yield the momentum distribution for dissociation.

The CE momentum spectra are obtained by first computing the ionization rate as the outgoing electron flux through $\pm z_{vd}$ at a given internuclear distance R. During the (fast) ionization of the electron we treat the (slow) nuclei as ''frozen.'' For each R, the Coulomb energy $1/R$ is released. In order to take the initial (dissociative) momentum

$$p_{\rm init}(R,t_i)=\left.\frac{\partial}{\partial R}\right|_{z_{vd}}\phi(z,R,t_i) \tag{16}$$

of the nuclei into account, we add the Coulomb energy and the initial kinetic energy of the nuclei at the ionization time and obtain the final momentum

$$p_R^{(\rm CE)}(R,t_i)=\sqrt{p_{\rm init}^2(R,t_i)+2\mu/R} \tag{17}$$

of the released fragments. Here, μ is the reduced mass of the nuclei. Analogous to the dissociation, integration over R and binning of the nuclear momentum values for all times t_i give the momentum distribution for CE.

III. RESULTS

Before we discus the vibrational-state dependence of the fragmentation of H_2^+ in a 25-fs laser pulse, we consider the intensity dependence for two selected vibrational states $|v=3\rangle$ and $|v=6\rangle$. The main difference between these states is the fact that $|v=3\rangle$ lies below the threshold for the 1ω

Floquet channel whereas states $|v=5\rangle$ or higher can decay into the 1ω as well as into the 2ω [29] channel that is open for all v states (see Fig. 1). Thus, lower v initial states need excited-state contributions $|v\geqslant 5\rangle$ in order to decay into the 1ω dissociation channel.

Vibrational excitation is likely in sufficiently short and intense laser pulses if the electric-field envelope changes significantly on the time scale of the vibrational motion. In this case, the time dependence of the dressed (Floquet) potential curves leads to nonadiabatic transitions between vibrational states. The influence of the pulse duration on the kinetic-energy spectra has been demonstrated by Frasinski *et al.* [18]. We note that these transitions are mediated by the interaction of the electron cloud with the laser field, since the nuclei cannot absorb photons directly. For all calculations, we used $\sin^2$ shaped 25-fs full width at half maximum pulses of 800-nm wavelength.

A. Fragmentation of H_2^+ ($v=3$) in a 25-fs laser pulse: Intensity dependence

Figure 3(a) shows the time-dependent norm

$$N(t)=\int_{0.05}^{R_{vd}} dR \int_{-z_{vd}}^{+z_{vd}} dz |\Psi(z,R,t)|^2 \tag{18}$$

and the probabilities for dissociation $D(t)$ and Coulomb explosion $C(t)$ for H_2^+ ($v=3$) interacting with a 25-fs laser pulse of intensity $I=0.2$ PW/cm^2. We find 20% probability for dissociation and 70% for CE. The time evolution of the nuclear probability density

$$P(R,t)=\int_{-z_{vd}}^{+z_{vd}} dz |\Psi(z,R,t)|^2 \tag{19}$$

is illustrated in Fig. 3(b) with contour lines indicating the electronic ionization rate due to CREI. In the density plot, the dissociation appears as a threefold jetlike structure. This structure can be associated with distinct peaks in the dissociation kinetic-energy spectrum shown as a solid line in Fig. 3(c) for intensities in the range from 0.05 to 0.5 PW/cm^2. The kinetic-energy range for one- and two-photon absorption into Floquet channels for all vibrational states is given by the shaded areas. For 0.1 PW/cm^2, we find the strongest dissociation. With increasing intensities, Coulomb explosion (dashed line) becomes dominant and results in the reduction of the final dissociation probability. At 0.2 PW/cm^2, the CE spectrum forms a broad peak between 4 and 8 eV corresponding to internuclear distances in the CREI region in Fig. 3(b) at $3.5\leqslant R\leqslant 7$. The CE peak is shifted towards higher kinetic energies for 0.5 PW/cm^2, showing a substructure which reflects the nodes of the initial wave function.

B. Fragmentation of H_2^+ ($v=6$) in a 25-fs laser pulse: Intensity dependence

Figure 4 shows the fragmentation dynamics of the $|v=6\rangle$ initial state. Compared to $v=3$, at 0.2 PW/cm^2 the dissociation probability is reduced to 10% and the CE enhanced to 88%. For the lower intensities, dissociation is much stronger than for the $|v=3\rangle$ initial state, mainly due to the opening of the 1ω channel [note the different scale in the upper row of Fig. 4(c)]. The CE spectra behave similarly to the $v=3$ case but with a generally higher ionization probability. The intensity dependence of the fragmentation (dissociation and CE) probabilities for the $|v=3\rangle$ and $|v=6\rangle$ initial states is summarized in Fig. 5. For $|v=3\rangle$, the dissociation channel shows a maximum of 37% around 0.1 PW/cm^2 whereas for $|v=6\rangle$ the dissociation probability increases further with decreasing intensity up to 73% at 0.05 PW/cm^2. The ionization (CE) probability reaches saturation for both initial states at 0.5 PW/cm^2.

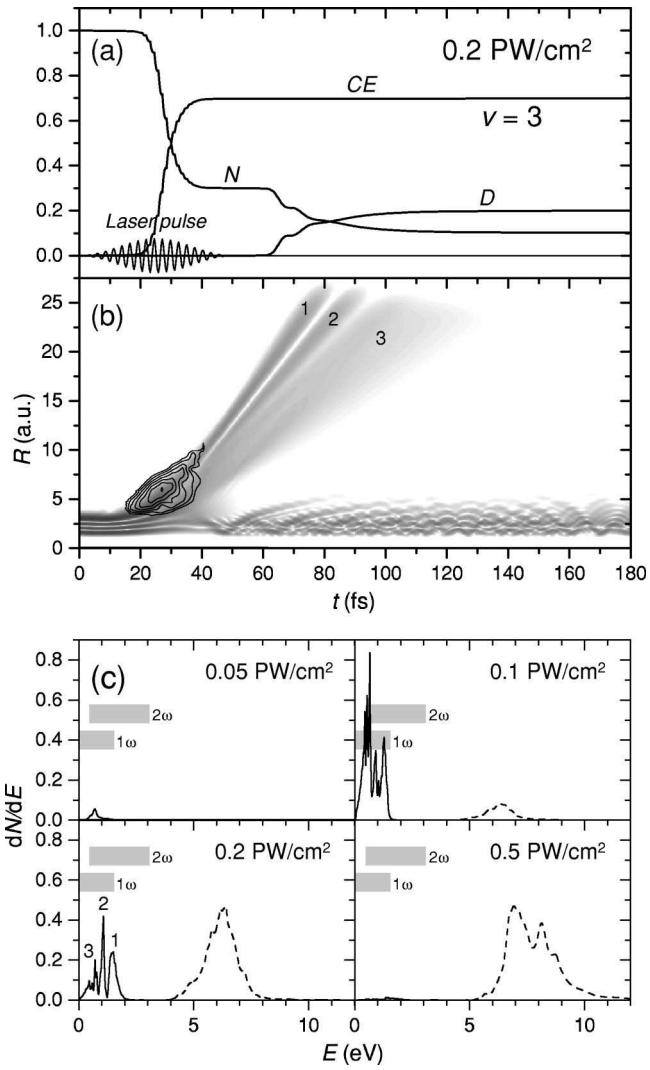

FIG. 3. Fragmentation of H_2^+ ($v=3$) in a 25-fs laser pulse. (a) Time-dependent norm (N) and probabilities for Coulomb explosion (CE) and dissociation (D) at $I=0.2$ PW/cm^2. (b) Corresponding probability density $P(R,t)$ (logarithmic gray scale) and ionization rates (contour lines). (c) Kinetic-energy spectra for dissociation (solid lines) and CE (dashed lines) for intensities in the range from 0.05 to 0.5 PW/cm^2.

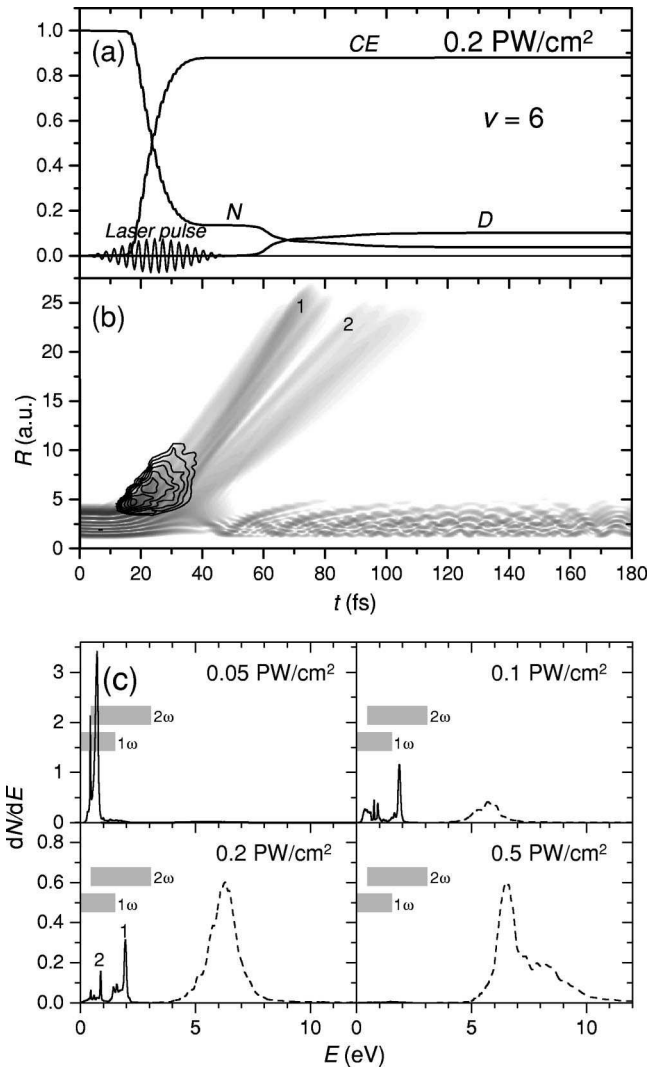

FIG. 4. Same as Fig. 3 but with $|v=6\rangle$ as initial state.

C. Fragmentation of H_2^+ in a 25-fs 0.2-P W/cm^2 laser pulse: Vibrational-state dependence

As mentioned above, for 25-fs pulses we have a competition of dissociation and CREI at an intensity of $\approx$0.2 PW/cm^2. Figure 6 shows the fragment kinetic-energy spectra for the initial states $|v\rangle$, $v=0-2$, 4, 5, 7–9 [for $v=3$, 6, see Figs. 3(c) and 4(c)]. These states significantly contribute to a Franck-Condon distribution one would expect for H_2^+ created in an ion source [24] (see Franck-Condon factors in Fig. 7). We find the vibrational ground state being almost stable against fragmentation. With increasing v, first dissociation dominates with a maximum probability of 33% for $|v=2\rangle$. Then CREI becomes more and more favorable at the expense of dissociation with ionization probabilities $>$90% for $|v=7\rangle$ and higher (see Fig. 7). There is also a noticeable shift in the dissociation spectra from the 1ω to the 2ω region (indicated by the shaded areas).

The v-dependent behavior of the ionization probability can be explained in the following way. For the low v states, we have first an expansion of the molecule due to bond softening. Once R reaches the ''critical'' region of 5–10, CREI becomes likely. With increasing v the overlap of the initial wave function with the CREI region becomes larger. In addition, these states are more sensitive to the bond softening. The increasing overlap of the initial states with the CREI

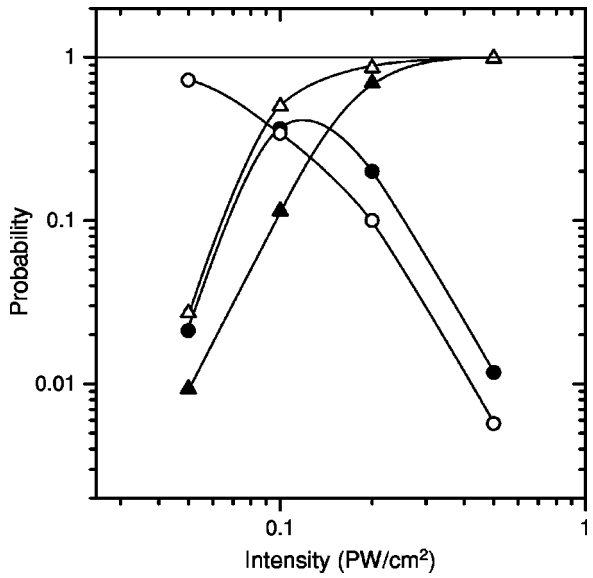

FIG. 5. Intensity dependence of the fragmentation probabilities. $|v=3\rangle$ initial state: ●, dissociation; ▲, CE. $|v=6\rangle$ initial state: ○, dissociation; △, CE. The curves joining the points only serve to guide the eye.

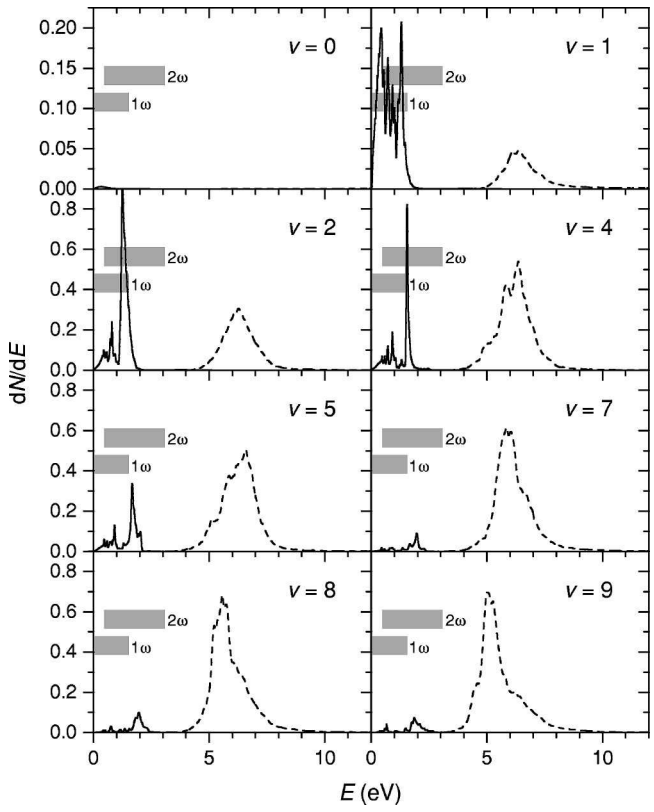

FIG. 6. Fragmentation of H_2^+ in a 25-fs laser pulse at $I=0.2$ PW/cm^2. Kinetic-energy spectra for dissociation (solid lines) and CE (dashed lines) for initial vibrational states $|v\rangle$, $v=0-2$, 4, 5, 7–9 [for $v=3$, 6 see Figs. 3(c) and 4(c)].

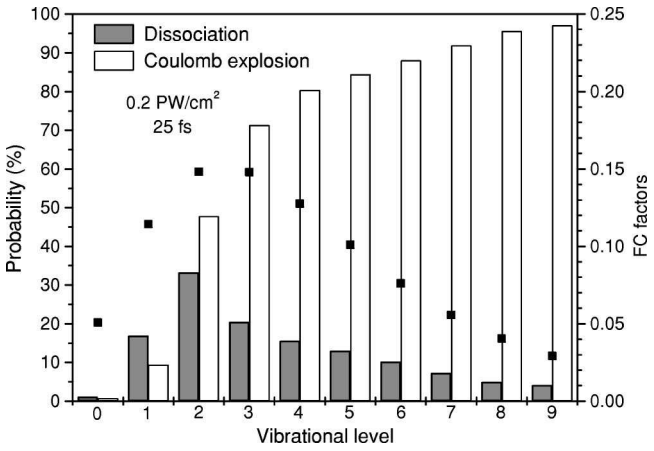

FIG. 7. Fragmentation of H_2^+ in a 25-fs laser pulse at $I = 0.2$ PW/cm^2. Initial-vibrational-state dependence of the probabilities for dissociation and CE. The black squares show the Franck-Condon factors (right scale) $|\langle H_2^+, v|H_2, v=0\rangle|^2$.

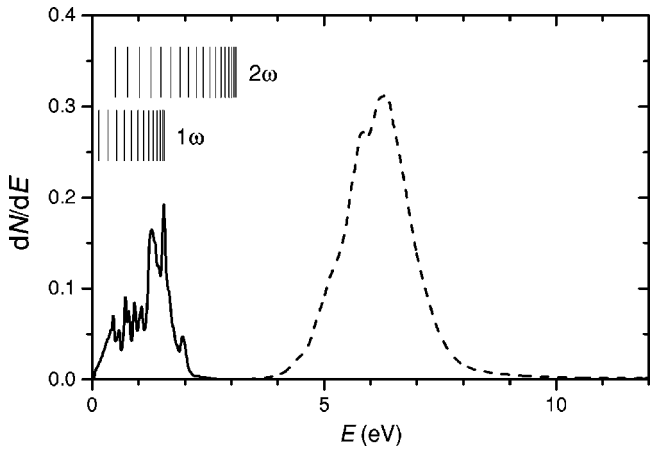

FIG. 8. Fragmentation of H_2^+ in a 25-fs laser pulse at $I = 0.2$ PW/cm^2. Kinetic-energy spectra for dissociation (solid lines) and CE (dashed lines) for a statistical (Franck-Condon) mixture of initial vibrational states.

region shifts the range where ionization occurs towards larger R. This results in lower Coulomb energy release, i.e., in a slight shift of the CREI peak in the spectrum from 6.5 eV ($v=1$) to 5 eV ($v=9$).

So far no experiment with selected pure initial vibrational states has been done due to technical difficulties. Ion sources usually provide a broad distribution of $|v\rangle$ states. The kinetic-energy spectrum for this kind of ensemble is shown in Fig. 8 for a 25-fs, 0.2-PW/cm^2 pulse. Here, we added the spectra for all significant states ($v=0,\ldots,9$), weighted with the Franck-Condon factors. As a result of this summation, much of the interesting v dependence is lost. An alternative to the preparation of pure states is the use of not too intense, ''long'' (>100 fs) pulses, which avoid nonadiabatic vibrational excitations. In this case, high-resolution spectroscopy allows the identification of individual $|v\rangle$ states in the 1ω and 2ω dissociation spectrum, as it has been done in the recent experiment by Sändig, Figger, and Hänsch [23].

IV. CONCLUSION

Using wave-packet propagation calculations within a collinear reduced-dimensionality model, we investigated the fragmentation of the H_2^+ molecular ion in 25-fs, 800-nm laser pulses in the intensity range 0.05–0.5 PW/cm^2. Our model represents both the nuclear and electronic motion by one degree of freedom including non-Born-Oppenheimer couplings. By introduction of a modified soft-core Coulomb potential for the electron-nucleus interaction with a softening function that depends on the internuclear distance, we were able to reproduce accurately essential properties of the ''real'' 3D molecule. We calculated the probabilities and kinetic-energy spectra for dissociation and CE of the molecule for various intensities and initial vibrational states. For the initial vibrational states $|v=3\rangle$ and $|v=6\rangle$ and different intensities, we demonstrated the effect of the threshold ($v \geqslant 5$) for the 1ω Floquet channel. For 0.2 PW/cm^2, our calculation revealed a strong vibrational-state dependence of the branching ratio between dissociation and CE. We found that dissociation dominates for molecular ions that are prepared in the two lowest vibrational states only, while CE becomes more and more dominant for higher vibrational states. The latter is caused by the increasing overlap of the initial nuclear wave function with the region of internuclear distances where CREI leads to high ionization probabilities. We also considered an incoherent (Franck-Condon) mixture of vibrational states, e.g., a beam of molecular ions created in an ion source. In contrast to a coherent superposition of vibrational states, the time dependence of which could be studied in a two-pulse pump-probe experiment [6], some of the interesting v dependence is lost after averaging over the Franck-Condon distribution. We hope that our work stimulates challenging future experimental investigations including the preparation of selected vibrational states.

ACKNOWLEDGMENTS

This work was supported in part by the National Science Foundation (Grant No. PHY-0071035) and the Division of Chemical Sciences, Office of Basic Energy Sciences, Office of Energy Research, U.S. Department of Energy. B.F. acknowledges the financial support from the Deutsche Forschungsgemeinschaft.

[1] M. R. Hermann and J. A. Fleck, Jr., Phys. Rev. A **38**, 6000 (1988).
[2] R. Kosloff, Annu. Rev. Phys. Chem. **45**, 145 (1994).
[3] K. C. Kulander, F. H. Mies, and K. J. Schafer, Phys. Rev. A **53**, 2562 (1996).
[4] S. Chelkowski, A. Conjusteau, T. Zuo, and A. D. Bandrauk, Phys. Rev. A **54**, 3235 (1996).
[5] A. G. Borisov, A. K. Kazansky, and J. P. Gauyacq, Phys. Rev.

B **59**, 10 935 (1999).
[6] B. Feuerstein and U. Thumm, Phys. Rev. A (to be published).
[7] U. Thumm, in *XXII International Conference on the Physics of Photonic, Electronic and Atomic Collisions, Santa Fe, New Mexico*, edited by S. Datz *et al.* (Rinton, Princeton, NJ, 2002), p. 592.
[8] T. Seideman, M. Y. Ivanov, and P. B. Corkum, Phys. Rev. Lett. **75**, 2819 (1995).
[9] T. Zuo and A. D. Bandrauk, Phys. Rev. A **52**, R2511 (1995).
[10] M. Plummer and J. F. McCann, J. Phys. B **29**, 4625 (1996).
[11] T. D. G. Walsh, F. A. Ilkov, S. L. Chin, F. Châteauneuf, T. T. Nguyen-Dang, S. Chelkowski, A. D. Bandrauk, and O. Atabek, Phys. Rev. A **58**, 3922 (1998).
[12] I. Kawata, H. Kono, and Y. Fujimura, J. Chem. Phys. **110**, 11152 (1999).
[13] D. Dundas, J. F. McCann, J. S. Parker, and K. T. Taylor, J. Phys. B **33**, 3261 (2000).
[14] Y. Duan, W.-K. Liu, and J.-M. Yuan, Phys. Rev. A **61**, 053403 (2000).
[15] M. E. Sukharev and V. P. Krainov, Phys. Rev. A **62**, 033404 (2000).
[16] G. N. Gibson, M. Li, C. Guo, and J. Neira, Phys. Rev. Lett. **79**, 2022 (1997).
[17] T. D. G. Walsh, F. A. Ilkov, and S. L. Chin, J. Phys. B **30**, 2167 (1997).
[18] L. J. Frasinski, J. H. Posthumus, J. Plumridge, K. Codling, P. F. Taday, and A. J. Langley, Phys. Rev. Lett. **83**, 3625 (1999).
[19] J. H. Posthumus, J. Plumridge, P. F. Taday, J. H. Sanderson, A. J. Langley, K. Codling, and W. A. Bryan, J. Phys. B **32**, L93 (1999).
[20] C. Trump, H. Rottke, and W. Sandner, Phys. Rev. A **59**, 2858 (1999); **60**, 3924 (1999).
[21] A. Staudte, C. L. Cocke, M. H. Prior, A. Belkacem, C. Ray, H. W. Chong, T. E. Glover, R. W. Schoenlein, and U. Saalmann, Phys. Rev. A **65**, 020703 (2002).
[22] H. Rottke, C. Trump, M. Wittmann, G. Korn, W. Sandner, R. Moshammer, A. Dorn, C. D. Schröter, D. Fischer, J. R. Crespo Lopez-Urrutia, P. Neumayer, J. Deipenwisch, C. Höhr, B. Feuerstein, and J. Ullrich, Phys. Rev. Lett. **89**, 013001 (2002).
[23] K. Sändig, H. Figger, and T. W. Hänsch, Phys. Rev. Lett. **85**, 4876 (2000).
[24] I. D. Williams, P. McKenna, B. Srigengan, I. M. G. Johnston, W. A. Bryan, J. H. Sanderson, A. El-Zein, T. R. J. Goodworth, W. R. Newell, P. F. Taday, and A. J. Langley, J. Phys. B **33**, 2743 (2000).
[25] Q. Su and J. H. Eberly, Phys. Rev. A **44**, 5997 (1991).
[26] B. Feuerstein and U. Thumm, J. Phys. B **36**, 707 (2003).
[27] W. H. Press, S. A. Teukolsky, W. T. Vetterling, and B. F. Flannery, *Numerical Recipes* (Cambridge University Press, Cambridge, 1992), p. 842.
[28] K. P. Huber and G. Herzberg, *Molecular Structure and Molecular Spectra IV. Constants of Diatomic Molecules* (Van Nostrand Reinhold, New York, 1979).
[29] We note that this channel corresponds to a *net* absorption of two photons. In fact, this channel exhibits first an absorption of three photons at the "3ω" crossing followed by a reemission of one photon at the subsequent "1ω" crossing (see also Fig. 1).